Small-scale Aeroelastic Rotor Simulation, Design and Fabrication

Paul Pounds, Robert Mahony
Australian National University, Canberra, Australia
paul.pounds@anu.edu.au, mahony@ieee.org

Abstract

Efficient, small-scale fixed-pitch rotor blades are essential for miniature rotorcraft. Extremely thin blade sections are required for highly efficient rotor performance that leads to acceptable mission endurance. Such rotor blades are difficult to manufacture from sufficiently rigid material to avoid significant torsional deformation in operating conditions. In practice, it is necessary to trade-off manufacturing simplicity and mechanical rigidity of a blade design against aerodynamic performance. This paper presents a design methodology for this problem, based on development of a simulator for steady-state rotor performance along with a search algorithm to find the ideal taper and twist geometry for a specified motor torque. The approach is demonstrated on the design of rotors for a small scale quad-rotor unmanned aerial vehicle under development at the Australian National University. Experimental thrust tests indicate good correspondence with theoretical predications.

Nomenclature

A	Rotor disc area, m^2
AoA	Angle of Attack, rad
c	Blade chord, m
c_d	Non-dimensional drag coefficient
c_l	Non-dimensional lift coefficient
c_m	Non-dimensional moment coefficient
$F.M.$	Figure of Merit
G	Material Shear Modulus, Pa
l	Blade element length, m
M	Blade section moment, Nm
q	Cross-sectional torque factor, m^4/rad
R	Rotor radius, m
RE	Reynold's Number
r	Blade radius station distance from axis, m
T	Rotor thrust, N
U	Blade linear velocity, m/s
V_i	Rotor inflow velocity, m/s
α	Blade angle of attack vector, rad
θ	Blade geometric angle vector, rad
κ	Blade twist angle, rad
ρ	Density of air, kg/m^3
τ	Torsional moment, Nm
υ	Ideal twist angle vector, rad
ψ	Pretwist angle vector, rad
ω	Rotor angular velocity, rad/s

1 Introduction

Unmanned Aerial Vehicles (UAVs) are rapidly becoming practical for an increasing variety of commercial applications. Current technology allows UAVs to track fires, monitor crop value and perform imaging tasks [UAVAC, 2005]. In addition to tasks that can be performed by fixed wing UAVs, rotary-wing aircraft can exploit their position-holding capabilities to do jobs such as scanning a dam wall for cracks or assessing powerline infrastructure [Golightly, 2002].

As the scope for commercial UAVs grows, logistical considerations in design and operation are becoming increasingly important. Mechanical simplicity is a crucial requirement for commercial UAV systems that will have to operate reliably and safely without regular skilled maintenance. The traditional helicopter configuration with a single main rotor requires a mechanically complex swash plate mechanism for actuation of collective and cyclic pitch (cf. Fig. 1) as well as a tail rotor system with collective pitch. The potential for catastrophic system failure due to poor maintenance is high. In contrast, a simple fixed-pitch rotor attached to a direct drive electric motor (cf. Fig. 1) has an almost negligible chance of catastrophic failure. For the X-4 Flyer under development at the Australian National University (ANU) [Pounds *et al*, 2004], the only moving parts are the four motor shafts with rigidly connected rotor assemblies.

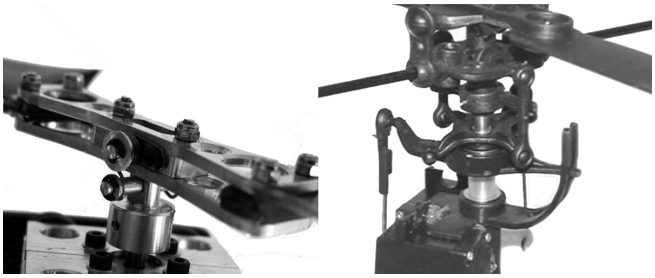

Figure 1: X-4 Flyer Mast and Conventional RC Heli Mast , Left and Right.

Small, custom-designed rotors can take advantage of ideal chord and twist geometry that is not practical for larger aircraft [Prouty, 2002, pp46]. However, optimal airfoils for low Reynold's Numbers are very thin and it is difficult to manufacture such blades. Moreover, the aerodynamic torque on the blades will cause them to deform under load conditions, a problem that is usually ignored in traditional helicopter systems where the variable pitch mechanism is used to adjust for changing angles of attack due to mechanical deformation of the blade. The design of high performance rotors for small scale UAVs is a trade-off between ease of manufacture, mechanical properties of the airfoil and optimal aerodynamic performance.

This paper proposes a method for calculating the steady-state torques on a rotor blade, the resulting elastic deflection and the change in aerodynamic performance. The mechanical qualities of the blade are derived from the material properties and the blade geometry. The aerodynamic performance of the blade is computed using classical steady-state fluid dynamics. The method is implemented with a simulator and optimisation algorithm. We apply the approach to the design of rotors for the ANU's X-4 Flyer. The manufacturing process used is an injection molded carbon fibre composite process using CNC-milled dies (cf. Fig. 2). In practice, it was necessary to modify the prototype thin section airfoils to improve the stiffness of the blades and ease of manufacture. Even with the blade profile modifications, the final aerodynamic design requires two to three degrees of pre-twist in the blade profile to ensure optimal angle of attack under operating conditions.

The paper is organised into five sections including the introduction. Section 2 discusses the key issues for the aerodynamic, mechanical and manufacturing design in detail. Section 3 describes the optimisation approach that we propose, along with details of the simulator program. Section 4 describes the design process for the X-4 Flyer in detail, while Section 5 provides a short conclusion.

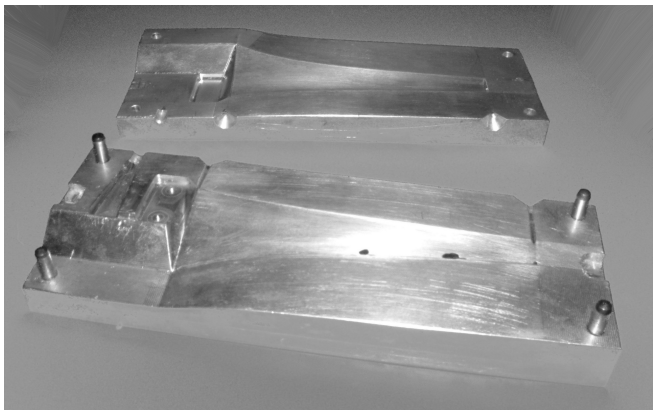

Figure 2: X-4 Flyer Blade Die.

2 Blade Design Trade-offs

The formulation of small-scale fixed-pitch blades is a trade-off between best aerodynamic design and best structural design. The goal of this process is to maximise the thrust produced at steady-state for a given mechanical power supplied to the rotor mast. For efficient thrust, the blade Angle of Attack (AoA) and Reynold's Number (RE) should be optimal for the airfoil. The blades must balance the aerodynamic moment due to lift with the elastic torque due to twisting, such that the airfoil operates in ideal conditions.

Under unbalanced aerodynamic load, the blade pitching moment increases the airfoil AoA: increasing angle leads to greater blade pitch moment (a positive feedback effect). If there is no restoring torque, the blades will twist until stall. As the blade twists, the torsional strain along the blade resists continued deformation. At the equilibrium angle, the aerodynamic bending moment will be exactly balanced by the elastic torque of the deforming blade. The goal of blade planform design is to regulate the geometric parameters so that the equilibrium angle is at the ideal AoA.

Only the steady-state aeroelastic effects are addressed. The unsteady elastic and aerodynamic effects are of the order of one rotor revolution [Leishman, 2000, pp369-371]. Even during highly aggressive manoeuvres of a UAV the unsteady aerodynamic effects will not have a significant impact on the rotor performance. A static analysis of the rotor performance will suffice for the purpose of design.

2.1 Aerodynamic Design

The best aerodynamic design is one that produces the most thrust in the flow regime encountered by the blade. For a typical small scale UAV, the RE is of the order of 100,000. In this regime it is expected that the fluid flow will be laminar [Potter, 1997, pp99] and the aerodynamics will be largely influenced by viscous effects.

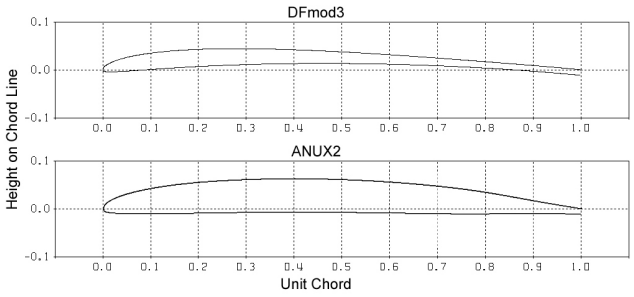

Figure 3: DFmod3 and ANUX2 Airfoil Sections, Top and Bottom.

The maximum length of the rotors will always be constrained by the geometry of the UAV and manufacturing limitations. Small blades need to rotate as fast as possible to generate the maximum thrust [Leishman, 2000, pp195-197]. The practical limitations on rotor speed are the motor drive torque and compressibility of air at the tip. Honnery [Honnery, 2000] gives Mach 0.3 as a practical tip velocity for avoiding compressibility effects.

The most efficient airfoil shape for these conditions is a high aspect-ratio blade section. Low camber and thin cross-section reduce profile drag; sharp trailing edges reduce separation drag. Example airfoils are DFmod3 (cf. Fig. 3, top) [Drela, 2003], VR8 and MA409sm [NASG, 2004].

Importantly, such airfoils may induce aerodynamic moments that dominate the torsional rigidity of the blade. To reduce the aerodynamic moment, the centre of pressure of the airfoil can be moved rearward. This is done by shifting the centre of thickness and camber away from the leading edge, such as in the ANUX2 airfoil (cf. Fig. 3, bottom). The moment generated by an airfoil can be made zero or even positive by adding 'reflex' near the trailing edge. However, reflexed airfoils typically have low lift coefficients [Hepperle, 2004]. The proposed airfoil is a trade-off between maximising lift and minimising moment.

Determination of the best airfoil is currently solved by humans using separate analytical tools, such as X-foil[Drela, 2004]. We used the simulator to provide comparative performance results for a series of airfoils and then chose the most promising, the ANUX2, for the design task. Once a prototype airfoil is chosen, the rotor geometry under operational load is obtained by optimising AoA, also denoted by α, and chord length at each radius station. Good blade design varies the geometric twist, θ, and chord along the blade, c, so that the AoA and RE are the ideal values at every point along the blade: $\theta = \alpha_{ideal} + V_i/\omega r$, cr = Constant, where V_i is the inflow velocity, ω is the rotor angular velocity, c is the chord and r is the radius. This is called 'ideal twist' and 'ideal taper', and is the theoretically optimal shape for hover [Prouty, 2002, pp46]. Structural constraints prohibit its use on large-scale helicopters, but small-scale rotors can readily apply it.

2.2 Structural Design

Mechanical stiffness of the rotor is crucial in reducing the angular deflection of the blade due to aerodynamic moments under operating conditions. Stiffness is improved by maximising material shear modulus, material bulk and torque factor, q, of the cross-sectional shape.

Shear modulus, G, is the key mechanical property in torsion [Roylance, 1996, pp74]. The blade material is chosen to maximise shear modulus along the blade axis. The fabrication and safety requirements of thin blade sections place limitations on the types of materials that can be used. Steel and titanium require large overheads to manufacture small sizes and high accuracy. Plastics are not sufficiently stiff for demanding performance. Composite materials offer good manufacturability and shear modulus, but risk stiffness variability due to hand-fabrication. We found carbon-fibre epoxy to be ideal for manufacturability and high shear modulus. Carbon-fibre fabric is anisotropic: the stiffness is at a maximum 45° to the weave [Roylance, 1996, pp114].

Typical high-lift airfoils are too thin to obtain sufficient structural strength. It is necessary to increase bulk to reduce the moment while attempting to preserve the blade's lift performance. This can be done by making the airfoil proportionally thicker in the body. The cross-sectional shape torque factor is dependent on the geometry of the airfoil cross-section [Roylance, 1996, pp78]. Material further out from the axis of twist counts for more than material on the axis. The torque factor can be increased by thickening the edges of the blade. However, adding thickness increases profile drag and so a trade-off between bulk and drag is necessary. We increase the material bulk of the ANUX2 airfoil by broadening the centre of thickness towards the leading and trailing edges.

The sensitivity of the steady-state angle to variation in the system attributes must also be considered. It is desirable to make the blade design tolerant of variations in the material stiffness or slop in the blade mounts. We account for this by applying a 'pre-twist' that sets the AoA lower so unexpected variations will have a greater strain margin before stall. If the system is accurately parameterised, the drag on the system will be lower; the rotor will run faster until the moment is balanced. We deliberately trade potentially higher thrust for robust operation. The stall sensitivity of the blade can be reduced by rounding the nose of the leading edge. This prevents early boundary layer seperation, allowing for a wider range of operating AoAs.

3 Blade Design Theory

The goal of the blade design is to maximise thrust. Analytically computing all the factors to generate the ideal geometry from first principles is difficult. The approach taken was to develop a simulator that computed the steady-state performance of a rotor for given geometric, aerodynamic and mechanical properties. The geometric properties were parameterised and an exhaustive search routine used to optimise the design for a aerodynamic and mechanical configuration. Finally, a range of airfoils were considered and insight from the simulated results, along with consideration of the manufacturability of the rotor, was used to design the proposed airfoil.

The purpose of the blade simulator is to determine the steady-state performance of a given blade shape for specified parameters:

- Motor and battery attributes

  The flux-linkage and internal resistances are used to calculate the torque output by the motor and and current drawn from the batteries. We used specified the maximum current draw to calculate drive torque for designing the X-4 Flyer rotors. Other design tasks have included a complete simulation of the motor electrical system.

- Material shear modulus, G

  The shear modulus of the material is used in computing the deflection of the blade under load. We keep this parameter constant for geometric design of the blades.

- Maximum tip speed, $\omega_{\max}$

  The maximum tip speed is limited to ensure the incompressible aerodynamics assumptions are valid. We use the maximum tip speed to set the design speed of the rotor – higher thrust will always be obtained with higher angular velocities.

- Airfoil polar data

  The algorithm is fed arrays of airfoil polar data. These tabulate non-dimensional lift coefficient, c_l, non-dimensional drag coefficient, c_d, and non-dimensional moment coefficient, c_m, over a range of AoAs, up to stall for specific REs. Due to the variable flow conditions, the simulator must be able to support a wide range of REs and AoAs. We use pre-generated polar tables at specified REs; airfoil performance data were derived entirely by simulation, using X-foil. This allows us to avoid the overhead in producing polars dynamically, but limits the resolution of RE and AoA tables. This is particularly pronounced in RE, where a data set may contain only a handful of explicitly calculated RE polars.

- Blade geometry $\theta(r)$, υ_{tip}, ψ, c_{tip}

  Blade geometry is given as a vector of angles, $\theta(r)$, and blade chords, $c(r)$, for a set of specified radius stations, r. We represent the ideal twist distribution by $\upsilon(r)$ and pretwist by $\psi(r)$ such that $\theta = \upsilon + \psi$. We denote ideal chord as $c_i(r)$. Specifying ideal tip angle, $\upsilon(R)$, and tip chord, $c_i(R)$, is enough to completely define $\upsilon(r)$ and $c_i(r)$.

The output of the simulator is the steady-state aerodynamic flow and the mechanical deformation of the blade. From the steady-state results we compute the following quantitative values:

- Thrust, T

  We use the overall thrust of the rotor to select the nominal 'best' rotor. The thrust required for lift places a lower limit on acceptable blade performance.

- Angular velocity, ω

  The steady-state velocity of the rotor is used to calculate shaft power and to check whether the blade tips are beneath the speed limit for incompressible fluid flow.

- Twist distortion vector, $\kappa(r)$

  The blade deflection vector, κ, is the elemental distortion at each radius station. When added to θ, it gives the loaded blade geometry for the steady-state flow conditions. We use it to determine how close the blade is approaching the ideal AoA.

- Figure of Merit

  Figure of Merit (F.M.) is a non-dimensional ratio that is the fraction of power induced in the air over power into rotor shaft. We use it as an efficiency of the rotor – a measure of how much power is being turned into work done on the air to generate thrust, versus the amount of power being output by the motor.

3.1 Simulation Algorithm

Each step of the simulator calculates the flow conditions of the rotor, aerodynamic moments, blade twist deflection, drag and the new angular velocity for the next step. At the end of each iteration the rotor state is checked for convergence.

To find the airfoil performance parameters, the angular velocity is used to calculate the RE each point along the blade. The airfoil polar table is searched for the nearest RE and AoA match, and the corresponding non-dimensional coefficients are returned.

The data are used to in blade element theory calculations to find the lift, drag and twist torque of each element. These are then summed along the blade to determine the total lift and drag over the whole rotor.

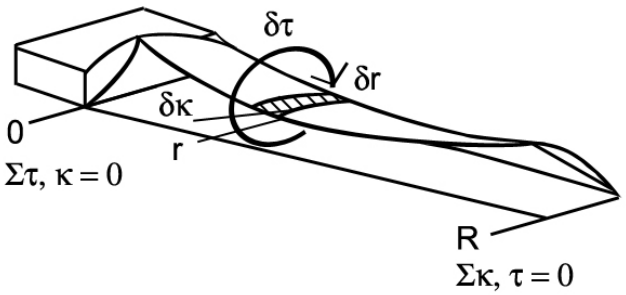

Figure 4: Balanced Aerodynamic Moment and Elastic Deformation Integrals.

Momentum theory is used to calculate the inflow velocity from the thrust produced, using $T = 2\rho A V_i^2$, where ρ is the density of air, and A is the area of the rotor disc [Seddon, 1996, pp6].

At steady-state, the aerodynamic and twist moments are balanced at all radius stations (fig. 4). The aerodynamic moment on a unit-length wing section is given by

$$M = c_m \frac{1}{2} \rho U^2 c^2 \tag{1}$$

where M is the moment, c_m is the non-dimensional moment coefficient, ρ is the density of air, U is the linear velocity and c is the chord length [Honnery, 2000, pp94, pp112]. The elastic deformation torque balance equation returns the differential twist over each blade element. The torque on a cross-section of length l is given by

$$\tau = \kappa \frac{Gq}{l} \tag{2}$$

where τ is the torque, κ is the strain angle, G is the material shear modulus and q is the torque factor. We approximate the torque factor of an airfoil by that of a flat plate of the same size.

The total aerodynamic moment acting at each radius station, r, of the blade is the integral of the aerodynamic moments inward from the tip to r. To satisfy the static torque equilibrium, this must be equal to the torque developed by the incremental twist at r.

$$\int_r^R c_m \frac{1}{2} \rho \left(\omega r\right)^2 \frac{c^2}{\delta r} dr = \delta\kappa \frac{Gq}{\delta r} \tag{3}$$

c_m is a function of AoA and r. The total deflection along the blade, κ, is the integral of the incremental twists from the root outwards. The geometric angle, θ, is invariant through the iterations.

At the end of the iteration, the speed, inflow and AoA are updated – new aerodynamic conditions will prevail and the process repeats for the next step. We take the difference between input torque and total drag torque to estimate the new rotor speed. The new speed is the angular velocity the rotor would reach with the available torque if the the flow and twist conditions were held constant. The new inflow is the the inflow calculated earlier. The blade AoA is recomputed with the new value of κ.

The simulator is run until the rotor torques and blade twist moments reach equilibrium. A recent history of rotor states is maintained so that convergence can be identified. The current state is tested against the stored states at the end of each step – if the previous speed and twist are identical to the current values, then the computation has converged.

The physical system must have a realisable steady-state. A limit cycle sometimes manifests in the calculations. We avoid this by introducing a damping effect into the state calculation. A weighted average with previous states causes cycles to decay. This slows down the rate of change of the parameters.

3.2 Search Routine

The outputs of the simulator are used by the search routine to identify the best input geometry. The search routine runs the simulator for a range of blade parameters and stores the results – this gives us a comprehensive picture of the blade performance space and sensitivity to blade characteristics. We used an automated search for maximum thrust with adjustments for robustness to choose our final configuration. The search variables are tip chord, ideal twist tip angle and a constant pretwist. The software used is available from Paul Pounds on request.

Ideally, the equilibrium state configuration would be one where the applied pretwist exactly negates the deformation at each radius station: $\theta = \upsilon + \psi + \kappa = \upsilon$. However, the range of pretwist configurations is very large and the gains from matching the inboard stations precisely is low. The majority of the lift is produced on the outboard third of the blades, and so we focus the optimisation on just the blade segments near the tip. At these radii, the moments are small and the ideal twist profile is roughly constant. Therefore, we approximate $\psi(r) = \text{constant}$.

This gives only three parameters for the search space: tip chord, tip angle and ψ. We discretised the space in each dimension to reduce the computational load, and so allowing a brute-force approach. Every incremental combination of the variables within reasonable ranges was computed and compared to find the highest thrust that robustly satisfied the design constraints. A search space of 0.5 to 2 mm chord in 0.1 mm increments, -2 to +4° ideal tip angle in 0.1° increments and -3 to +1° pretwist angle in 0.05° increments completed overnight running in Matlab on a 2.8 MHz computer.

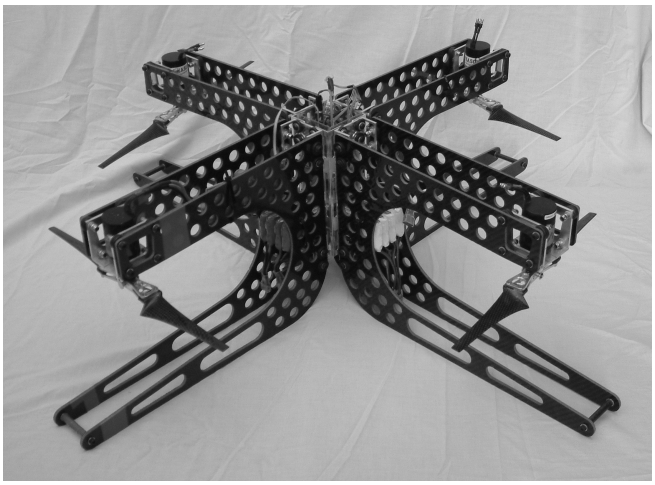

Figure 5: Australian National University X-4 Flyer.

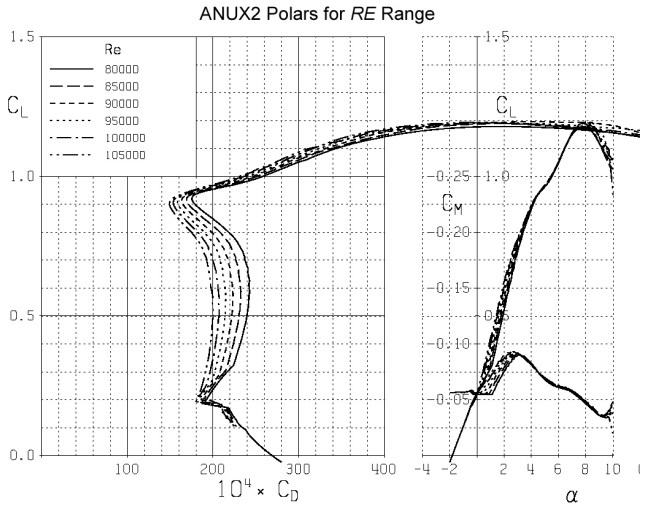

Figure 6: ANUX2 Polar Plot.

4 Rotor Design for X-4 Flyer

The ANU X-4 Flyer (cf. Fig. 5) was conceived as a platform for use in visual servo control experiments [Pounds *et al*, 2002]. Unlike smaller research quad-rotors, it is designed to carry a significant and variable payload. The flyer is intended to be used indoors, but is also expected to be robust enough to fly outdoors. The target weight of the flyer is 4 kg total, with 0.5 to 1 kg payload. It should have a flight time greater than 10 minutes.

Initial tests with off-the-shelf hobby propellers showed that properly engineered rotors are essential for practical performance [Pounds *et al*, 2002]. We used the simulator to design rotors matched to the hardware available and anticipated flight condition.

4.1 Hardware

The drive components selected were Jeti Phasor 30-3 brushless motors, along with custom electronic speed controllers. A particular advantage of this motor is the high torque performance that allows for direct drive of the rotors, rather than requiring gearing. The motors can pass more than 300 W at a maximum of 35 A.

Power is provided by Kokam 1500 mAh high-discharge cells. Each cell is nominally rated at 3.7 V and can deliver 12 A constantly, or 15 A for short bursts. The batteries are connected to a power bus of eight parallel sets of four cells in series; that is, 14.8 V nominal voltage and 24 A of current draw per motor.

4.2 Requirements and Blade Design

For a quad-rotor helicopter weighing 4 kg with a 30 per cent control margin, each motor must produce 12.7 N of thrust. The rotor radius can be no greater than 0.165 m, due to the size of the robot. This will require 101.2 W of power induced in the air. The rotational velocity should ideally be less than 800 rads^{-1} to avoid compressibility effects at the blade tip. The battery current limit of 22 A produces a maximum 0.1749 Nm motor torque and hence a top shaft power of 131 W. Therefore, the maximum theoretical thrust is 15.1 N per motor (assuming $F.M. = 1$). The actual rotor design $F.M.$ must be no less than 0.77.

The appropriate airfoil for this flight regime is a high lift, low speed design. It should be insensitive to small changes in AoA and demonstrate good performance over the operating RE range. A variety of high-lift, low-speed airfoils were tested in the aeroelastic simulator and the best chosen for detailed analysis. None of these airfoils satisfied all the requirements of the design specification and so a new cross-section was developed.

The 'ANUX2' (ANU X-4 airfoil v2) (cf. Fig. 3, bottom) is a custom airfoil specially suited to the X4. The design was obtained by progressively modifying an example high-lift airfoil, the Dfmod3 (cf. Fig. 3, top), to satisfy mechanical and manufacturing requirements. The ANUX airfoils are relatively thick in the body to improve bulk and torque factor. They have a broad nose to reduce stall sensitivity. The bottom surface is flat to increase thickness and improve manufacturability (cf. Fig. 3, bottom). The centres of camber and thickness are towards the aft to reduce c_m. The ANUX2 operates most efficiently at $RE = 94,000$ with an ideal AoA of 4.4° (cf. Fig. 6). The ANUX2 demonstrated superior performance to the DFmod3, VR8 and MA409sm in the aeroelastic simulator. It has a good c_l of 0.9, 7 per cent thickness ratio and significant bulk towards leading and trailing edges.

For the ANUX2, the optimal geometry was a tip chord of 10.4 mm and tip pitch of 3.9°, given ideal pitch and

u/units	$V_0 \pm 0.1$/V	$V \pm 0.1$/V	$I \pm 0.1$/A	$\omega\pm$/rads^{-1}	$T \pm 0.05$/N
50	15.4	14.9	1.2	326	1.35
75	15.4	14.5	2.2	429	2.46
100	15.2	13.8	4.3	534	3.52
125	15.1	13.4	6.6	634	5.05
150	15.1	12.8	10.9	722	6.53
175	15.0	12.0	13.4	775	7.74
			Battery change		
185	16.1	13.7	–	921	11.16
200	16.8	12.9	–	926	11.24
225	16.6	12.7	–	1015	13.63
250	16.3	11.7	–	1043	14.53

Table 1: Static Rotor Performance.

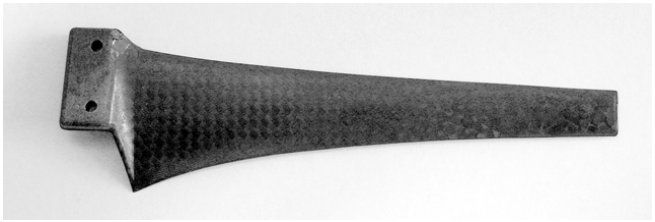

Figure 7: ANUX2 Blade With Ideal Chord.

chord. The simulator calculated a total thrust of 13.87 N at 764 rads^{-1}. The length of the blade is 165.1 mm (from the shaft centre), with the hub clamp at 40 mm. It is not possible to reduce the bulk of the airfoil without compromising the rigidity of the blade.

Remark. We found that the screw-down mounting bracket was not accurate to more than 0.5°. For the production blade (cf. Fig. 7), the tip angle was reduced to 3.1° to allow for any unexpected flex or angular error; simulation showed that variations of as much as 2° in mounting pitch error could still produce sufficient thrust. If there is no slop or flexural variation, the motor will just run faster before reaching equilibrium.

4.3 Experimental Results

Thrusts tests were run to assess the performance of the blades. The apparatus consisted of a Jeti motor mounted on the flyer, which is fixed on a teetering rig. The other side of the flyer pressed down on a digital scale. During each test, the motor speed and power data were logged from the speed controller and the digital scale was read directly.

The rotor produced more than 14 N of thrust at full speed, as shown in (cf. Tab. 1)[1], comparing favourably with the simulator prediction (+5 per cent). It was found that the actual blades run faster than predicted. We suspect this is because the estimated shear modulus of carbon-fibre was less than that of the actual material. This resulted in a lower AoA and less induced drag.

Current draw measurements from previous tests [Pounds *et al*, 2004] give the X-4 a theoretical endurance of more than eight minutes at constant full throttle. From simulation, the motor is expected to draw 16.9 A at hovering speed, and this flight-time could be extended to beyond 10 minutes. When used on the X-4 Flyer UAV, the rotors were capable of lifting the helicopter, but actual flight time performance has not been tested.

The difference in performance from the expected value may result from inaccuracies in the leading and training edges introduced by hand-trimming of the injection molded parts. The rotor was raised one rotor diameter (0.33 m) off the ground, but may still experience aerodynamic interference.

5 Conclusion

We have introduced a method for designing small rotors suitable for high-performance UAV applications. The method uses a mix of blade element theory, momentum theory and element-wise torsion analysis to determine the aeroelastic behaviour of the blade in steady state.

A successful design must incorporate considerations including airfoil performance, ideal taper, blade stiffness, manufacturability and sensitivity to variation. It is possible to test a specified blade geometry in the simulator to determine steady-state thrust and speed at given conditions. A simple search algorithm can identify the optimal rotor geometry for an expected flight envelope.

This process was used to develop blades for the ANU's X-4 Flyer. The actual blades performed better than predicted and are each capable of lifting approximately 1.5 kg of weight.

1. The current sensor function of the boards was not calibrated for the entire operating range and saturated at 13.8 A.

References

[UAVAC, 2005] UAV Applications Center. *UAV Applications Projects.* http://www.uav-applications.org/projects.html, August 2005.

[Drela, 2004] M. Drela. X-Foil Subsonic Airfoil Development System. http://raphael.mit.edu/xfoil/, August 2004.

[Drela, 2003] M. Drela. *MIT 16.82 Flight Vehicle Engineering Course Demonstrator.* http://student.mit.edu/catalog/m16b.html, 2004.

[Golightly, 2002] I. Golightly and D. Jones. *Visual Control of an Unmanned Aerial Vehicle for Power Line Inspection.* IEEE Int Conf Advanced Robotics (ICAR 2005), 2005, Seattle, USA, pp. 288-295.

[Hepperle, 2004] M. Hepperle. *Airfoils for Tailless Airplanes.* www.mh-aerotools.de/airfoils/nf_1.htm, August 2004.

[Honnery, 2000] D. Honnery. Introduction to the Theory of Flight. Gracie Press, Northcote, Victoria, 2000.

[Leishman, 2000] J. Gordon Leishman. Principles of Helicopter Aerodynamics. Cambridge University Press, Cambridge, United Kingdom, 2000.

[NASG, 2004] Nihon University Aero Student Group. *Airfoil Database.* www.nasg.com/afdb/index-e.phtml, August 2004.

[Potter, 1997] M. Potter and D. Wiggert. Mechanics of Fluids. Prentice-Hall, Inc., Upper Saddle River, New Jersey, 1997.

[Pounds *et al*, 2002] P. Pounds, R. Mahony, P. Hynes and J. Roberts. *Design of a Four-Rotor Aerial Robot.* In *Proc. of Australasian Conference on Robotics and Automation*, Auckland, New Zealand, 2002.

[Pounds *et al*, 2004] P. Pounds, R. Mahony, J. Gresham, P. Corke, J. Roberts. *Towards Dynamically-Favourable Quad-Rotor Aerial Robots.* In *Proc. of Australasian Conference on Robotics and Automation*, Canberra, Australia 2004.

[Prouty, 2002] R. W. Prouty. Helicopter Performance, Stability, and Control. Krieger Publishing Company, 2002, reprint with additions, original edition 1986.

[Roylance, 1996] D. Roylance. Mechanics of Materials. John Wiley & Sons Inc., New York, 1996.

[Seddon, 1996] J. Seddon. Basic Helicopter Aerodynamics. Blackwell Science, Osney Mead, Oxford, 1996.

[Wells, 2004] V. Wells. *Propeller.* www.eas.asu.edu/~harvee/papers/propeller.pdf, August 2004.